Supporting Information

Baxter et al. 10.1073/pnas.0910333106

SI Text

Materials. All chemicals were obtained from Sigma except the G6P analogue, 6-deoxy-6-(phosphonomethyl)-D-glucopyranoside, which was synthesized as described previously (1).

Methods. ***Crystallization of native β-PGM and the PGM-MgF_3-G6P-TSA complex.*** For the crystallization experiments of native β-PGM and the PGM-MgF_3-G6P-TSA complex, frozen unlabeled β-PGM, expressed and purified as detailed previously (2) was thawed and the buffer exchanged to one containing 50 mM K^+ Hepes pH 7.2, 5 mM $MgCl_2$, 1 mM NaN_3 and 0.1 mM DTT. For the PGM-MgF_3-G6P-TSA complex, 10 mM NH_4F and 5 mM G6P were added. Solutions were then adjusted to a protein concentration of 15 mg · mL^{-1}. Initial crystallization conditions were found at the High Throughput Crystallisation Laboratory, the Partnership for Structural Biology, Grenoble, France. For crystallization of the PGM-MgF_3-G6P-TSA complex, 2 μL of the solution defined above was mixed 1:1 with the precipitant (19–21% PEG 3350, 50 mM magnesium acetate and 1 mM deferoxamine to chelate any contaminating aluminum) and placed in sitting drop crystallization plates. Large plate crystals appeared after 1 week and had the approximate dimensions 0.5 mm × 0.1 mm × 0.1 mm. For cryoprotection, the crystals were transferred to a buffer containing 22% PEG 3350, 50 mM magnesium acetate, 10 mM NH_4F, 10 mM G6P, 5 mM $MgCl_2$, 1 mM deferoxamine, 50 mM K^+ Hepes pH 7.2 and 5% PEG 400 (v/v). The PEG 400 concentration was increased to 20% (v/v) in 5% steps (15 min at each concentration) by transferring the crystals between buffers with an increasing concentration of PEG 400. Crystals were harvested with a mounted LithoLoop (Molecular Dimensions Ltd.), plunged into liquid nitrogen and stored at 100 K. For crystallization of the native (open conformation) β-PGM, 2 μL of the protein was mixed 1:1 with the precipitant (26–30% PEG 4000, 200 mM sodium acetate, and 100 mM Tris pH 7.5) and placed in sitting drop crystallization plates. Small needle crystals appeared after 2 days with the approximate dimensions 0.03 mm × 0.05 mm × 0.5 mm and had different cell dimensions to the PGM-MgF_3-G6P-TSA complex (Table S1). Crystals were cryoprotected by transferring them to a buffer containing 32% PEG 4000, 200 mM sodium acetate, 100 mM Tris pH 7.5, 5 mM $MgCl_2$, and 5% PEG 400 (v/v). Again the PEG 400 concentration was increased to 20% in 5% steps by the transfer of crystals between buffers.

Data collection and refinement. Diffraction data were collected from cryocooled crystals to between 1.55 Å and 1.3 Å resolution on an ADSC Q210 CCD detector on beamline ID14-2 ($\lambda = 0.933$ Å) at the European Synchrotron Radiation Facility, Grenoble, France (Table S1). A long-wavelength dataset was collected to 2.0 Å on a crystal of the PGM-MgF_3-G6P-TSA complex at a wavelength of 1.77 Å ($E = 7$ keV) at beamline ID29 on an ADSC Q315 CCD detector in order to exploit the anomalous signal from phosphorus at this wavelength (3). A wide ϕ range (320°) was collected to have a high redundancy to increase the anomalous signal. Data were processed with MOSFLM (4) and programs from the Collaborative Computational Project Number 4 suite (5). The structures were solved by molecular replacement with MolRep (6) using PDB accession code 1o08 (7) as a search model for the PGM-MgF_3-G6P-TSA complex and PDB accession code 1zol (8) for the native conformation with all ligands and water molecules removed in both cases. In all subsequent refinement steps, 5% of the data were excluded for calculating the free R-factor. Refinement was carried out alternately with REFMAC5 (9) and by manual rebuilding with the program COOT (10). Some solvent molecules were built with the ARP/waters function of ARP/wARP (11). Ligands were not included until the final rounds of refinement so they could be built into unbiased difference Fourier maps. For the final round of refinement, restraints for the MgF_3^- moiety were relaxed allowing the exact atomic positions to be defined. Stereochemistry was assessed with COOT (10) with all residues in preferred or allowed regions. Figs. 2*A* and 3*A* and *B* and Figs. S3–S5 were produced with PyMol (12).

Both complexes crystallized in the orthorhombic space group $P2_12_12_1$ with one molecule in the asymmetric unit but with varying unit cell dimensions and the statistics are summarised in Table S1. The models contain the following residues: PGM-MgF_3-G6P-TSA complex; 1–218 and native β-PGM: 1–221. The maps for all the structures were of excellent quality with only one loop region (approximately residues 59 to 64) being slightly disordered in the PGM-MgF_3-G6P-TSA complex structure. After one round of refinement clear difference density was visible for the sugar phosphate and metal fluoride moiety. Omit maps for the ligands are shown in Figure S3. The difference Fourier maps were extremely clear for all ligands. In the native β-PGM structure clear difference density for a magnesium ion coordinated to D8, D170 and E169 was visible. No density for a phosphorylated aspartate residue was visible (Fig. S1).

Refinement of structure 1o08. Deposited coordinates and structure factors for 1o08 were downloaded from the PDB (www.pdb.org) and a dictionary for β-glucose 1,6-bisphosphate bond length and angle restraints was obtained from the HIC-Up website (13). The model was subjected to 10 cycles of restrained anisotropic refinement using REFMAC5 (9) with resulting *R* factors that were similar to those reported (7) before maps were calculated. In order to compare the refinement of the proposed pentacovalent phosphorane with the alternative interpretation of a PGM-MgF_3-G6P-TSA complex, a model containing G6P as the only bound ligand was refined against the structure factors. MgF_3^- was then built into the resulting difference Fourier maps showing a trigonal planar species and the model subjected to a further 10 cycles of anisotropic refinement. The atoms of the MgF_3^- were not restrained during refinement. The resulting electron density maps are shown in Figs. 3*B* and S5.

^{19}F and ^{31}P 1D NMR experiments. Unlabeled and ^{15}N-labeled β-PGM was expressed and purified as detailed previously (2). Initially, a ^{31}P spectrum (with a two minute dead-time) was acquired at 291 K on a sample of β-PGM containing 0.5 mM unlabeled β-PGM, 10 mM $MgCl_2$, 5 mM G6P, 1 mM DTT, 1 mM K^+ Hepes buffer pH 7.5, which replicated the conditions reported in the crystallization studies (7), except that 100 mM NH_4F was omitted. For the ^{31}P experiments acquired on the PGM-MgF_3-G6P-TSA complex at 298 K, the sample contained 2 mM unlabeled β-PGM, 5 mM $MgCl_2$, 10 mM NH_4F, 5 mM G6P, 2 mM NaN_3, in 50 mM K^+ Hepes buffer pH 7.2 with 10% D_2O present internally for the lock. Spectra were recorded on a Bruker Avance 500 MHz spectrometer fitted with a broadband probe tuned to ^{31}P (202.45 MHz). A total of ~48,000 transients were acquired with ^1H decoupling over a spectral width of 100 ppm and the spectra were processed with 5 Hz Lorentzian apodization. For the ^{19}F NMR experiments at 298 K, samples were prepared separately in both 50 mM K^+ Hepes buffer in 100% H_2O pH 7.2

and 50 mM K^+ Hepes buffer in 100% D_2O pH 7.2 (uncorrected for D_2O effects) and contained 0.5 mM unlabeled β-PGM, 5 mM $MgCl_2$, 10 mM NH_4F, 2 mM NaN_3, and either 5 mM G6P (PGM-MgF_3-G6P-TSA), 5 mM 2-deoxy-G6P (PGM-MgF_3-2deoxyG6P-TSA) or 5 mM 6-deoxy-6-(phosphonomethyl)-D-glucopyranoside (PGM-MgF_3-phosphonate-TSA). In the 100% H_2O buffer experiments, the lock was provided by D_2O sealed inside a capillary inserted in the NMR sample tube. The spectra were recorded on a Bruker Avance 500 MHz spectrometer (operating at 470.59 MHz for fluorine) equipped with a dual $^1H/^{19}F$ probe. Typically, ~64,000 transients were acquired without ^1H decoupling over a spectral width of 100 ppm and were processed with sinebell functions shifted by 60°.

Measurement of K_d values by ^1H NMR. The effective K_d values for the sugar phosphates in the PGM-MgF_3-2deoxyG6P-TSA and PGM-MgF_3-phosphonate-TSA complexes were determined at 298 K by ^1H 1D NMR spectra using a Bruker Avance 800 MHz spectrometer equipped with a $^1H/^{15}N/^{13}C$ probe and z-axis gradients. Stock solutions (50 mM) of the sugar phosphates were prepared separately in 50 mM K^+ Hepes buffer pH 7.2 containing 5 mM $MgCl_2$ and 10 mM NH_4F. These solutions were titrated serially into protein solutions containing 0.5 mM ^{15}N-labeled β-PGM, 5 mM $MgCl_2$, 10 mM NH_4F, 1 mM NaN_3, in 50 mM K^+ Hepes buffer pH 7.2 with 10% D_2O present internally for the lock. Successive decreasing integral values of well-dispersed peaks in the ^1H NMR 1D spectra characteristic of open native β-PGM were obtained as a function of increasing sugar phosphate concentrations and K_d values were calculated using a least-squares fitting algorithm corrected for dilution effects.

Measurement of K_d values by isothermal titration calorimetry. The effective K_d value for G6P in the PGM-MgF_3-G6P-TSA complex was determined using a VP-ITC (MicroCal,) equilibrated at 25 ° C. A β-PGM solution (10 μM, 2 mL) and a G6P stock solution (100 μM, 1 mL) were separately equilibrated in 50 mM K^+ Hepes buffer pH 7.2 supplemented with 5 mM $MgCl_2$ and 10 mM NH_4F. Binding isotherms were obtained by the titration of the G6P stock solution (18 injections, 15 μL each) into the β-PGM solution and were continued beyond saturation levels. Heats of ligand dilution were obtained by the titration of the G6P stock solution (18 injections, 15 μL each) into the above buffer prepared in the absence of protein. Following the subtraction of the heats of dilution, the resulting data were fitted to a single-site binding isotherm using the ORIGIN software supplied with the calorimeter.

Measurement of J_{HF} and J_{NF} couplings. ^1H, ^{15}N HSQC experiments were recorded without ^{19}F decoupling on the PGM-MgF_3-sugar phosphate-TSA complexes, using samples prepared as above except that 0.5 mM ^{15}N-labeled β-PGM was used and 10% D_2O was present internally for the lock. The sugar phosphate was 10, 100, and 50-fold in excess of β-PGM for the G6P, the 2deoxyG6P and the 6-deoxy-6-(phosphonomethyl)-D-glucopyranoside complexes, respectively. The spectra were acquired at 298 K on a Bruker Avance 500 MHz spectrometer equipped with a $^1H/^{15}N/^{13}C/^{19}F$ probe and z-axis gradients. The identity of the coupling partner as ^{19}F was established using ^{19}F decoupling implemented by the insertion of a composite 180° pulse in the indirect ^{15}N acquisition delay and by composite pulse decoupling during the direct ^1H acquisition. On-resonance decoupling was activated by adjusting the ^{19}F frequency to −149 ppm (approximate average of $F_A = -147.0$ ppm and $F_B = -151.8$ ppm). Where resonance overlap in the HSQC spectra restricted the observation of components of the ^{19}F-coupled H-N crosspeak, spectral editing was achieved via the stimulation of truncated-driven NOEs between fluorine nuclei and their J-coupled partners. Proton chemical shifts were referenced relative to the methyl signals of internal DSS at 0.0 ppm. ^{15}N, ^{31}P and ^{19}F chemical shifts were calculated indirectly by using the following gyromagnetic ratios: $^{15}N/^1H = 0.101329118$, $^{31}P/^1H = 0.404807356$ and $^{19}F/^1H = 0.940940080$. All NMR data were processed, analyzed, and interpreted using FELIX (Felix NMR Inc, San Diego, CA).

1. Berkowitz DB, Bose M, Pfannenstiel TJ, Doukov T (2000) α-Fluorinated phosphonates as substrate mimics for glucose 6-phosphate dehydrogenase: the CHF stereochemistry matters. *J Org Chem* 65:4498–4508.
2. Baxter NJ, Olguin LF, Goličnik M, Feng G, Hounslow AM, Bermel W, Blackburn GM, Hollfelder F, Waltho JP, Williams NH (2006) A Trojan horse transition state analogue generated by MgF_3^- formation in an enzyme active site. *Proc Natl Acad Sci USA* 103:14732–14737.
3. Mueller-Dieckmann C, Panjikar S, Schmidt A, Mueller S, Kuper J, Geerlof A, Wilmanns M, Singh RK, Tucker PA, Weiss MS (2007) On the routine use of soft x-rays in macromolecular crystallography. Part IV. Efficient determination of anomalous substructures in biomacromolecules using longer x-ray wavelengths. *Acta Cryst* D63:366–380.
4. Leslie AGW (1992) Recent changes to the MOSFLM package for processing film and image plate data. *Joint CCP4 and EACMB Newsletter on Protein Crystallography* 26, Daresbury Laboratory, Warrington, United Kingdom.
5. Collaborative Computational Project Number 4. (1994) The CCP4 suite: Programs for protein crystallography. *Acta Cryst* D50:760–763.
6. Vagin A, Teplyakov A (1997) *MOLREP*: an automated program for molecular replacement. *J Appl Cryst* 30:1022–1025.
7. Lahiri SD, Zhang G, Dunaway-Mariano D, Allen KN (2003) The pentacovalent phosphorus intermediate of a phosphoryl transfer reaction. *Science* 299:2067–2071.
8. Zhang G, Dai J, Wang L, Dunaway-Mariano D, Tremblay LW, Allen KN (2005) Catalytic cycling in β-phosphoglucomutase: A kinetic and structural analysis. *Biochemistry* 44:9404–9416.
9. Murshudov GN, Vagin AA, Dodson EJ (1997) Refinement of macromolecular structures by the maximum-likelihood method. *Acta Cryst* D53:240–255.
10. Emsley P, Cowtan K (2004) Coot: model-building tools for molecular graphics. *Acta Cryst* D60:2126–2132.
11. Lamzin VS, Wilson KS (1993) Automated refinement of protein models. *Acta Cryst* D49:129–147.
12. DeLano WL (2002) The PyMOL Molecular Graphics System. DeLano Scientific, San Carlos, CA, USA.
13. Kleywegt GJ (2007) Crystallographic refinement of ligand complexes. *Acta Cryst* D63:94–100.

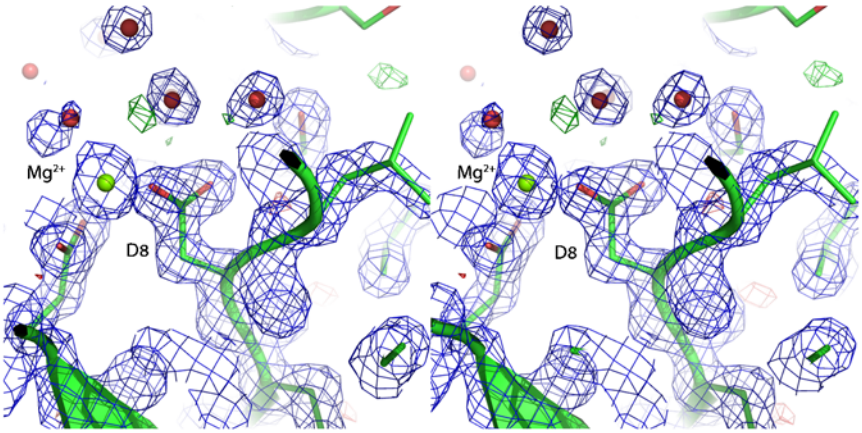

Fig. S1. Stereoview of the native β-PGM structure active site. The protein Cα chain is shown as a ribbon and residues D8 and E169 are shown as sticks. $2F_o - F_c$ density is shown as a *blue mesh* contoured at 1.5σ, difference density ($F_o - F_c$) is shown as *green and red meshes* contoured at +3σ and −3σ, respectively. No density was observed for an aspartyl phosphate.

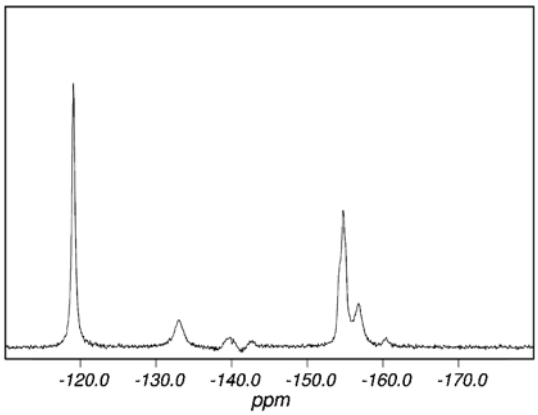

Fig. S2. ^{19}F NMR spectrum of β-PGM complexed with aluminum fluoride. The sample contained 0.5 mM β-PGM, 5 mM $MgCl_2$, 10 mM NH_4F, 1 mM $AlCl_3$ and 1 mM NaN_3 in 50 mM K^+ Hepes buffer pH 7.2 with a capillary containing D_2O inserted in the NMR tube present for the lock. The spectrum was acquired using the methods described. The four peaks corresponding to protein-bound aluminum fluoride resonances have the following ^{19}F chemical shifts: −133, −140, −143 and −160 ppm. The peak at −119 ppm corresponds to free F^- and those at −155 and −157 ppm are from free AlF_x species.

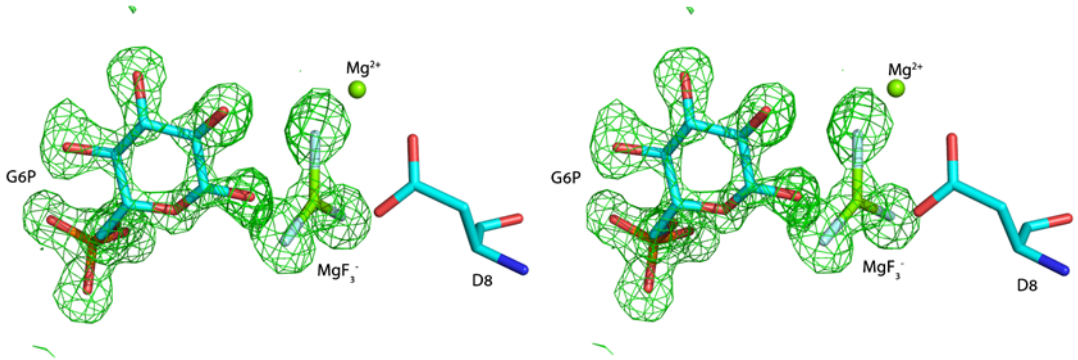

Fig. S3. Stereoview of the difference Fourier maps for the active site of the PGM-MgF_3-G6P-TSA complex. Difference density ($F_o - F_c$) for G6P and MgF_3^- is shown as a *green mesh* contoured at 3σ before their inclusion in the model. The MgF_3^- moiety is coordinated between O1 of the sugar phosphate and the catalytic aspartate (D8) of β-PGM.

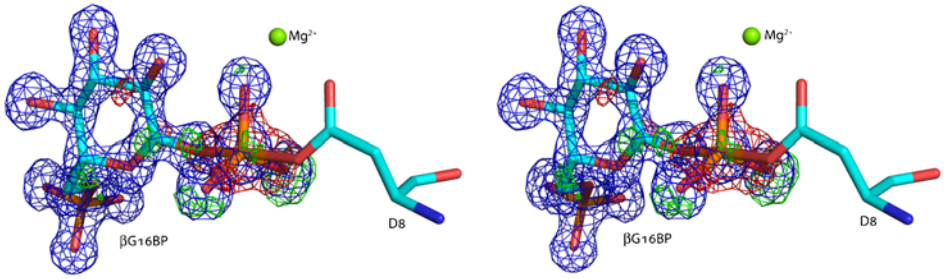

Fig. S4. Stereoview of the electron density maps for the β-PGM active site in 1o08. Coordinates and structure factors were downloaded and refined as described in methods. $2F_o - F_c$ density is shown as a *blue mesh* contoured at 1.5σ, difference density ($F_o - F_c$) is shown as *green and red meshes* contoured at +3σ and −3σ, respectively. Positive peaks (*ca*. 8σ) are observed beyond each of the equatorial atoms of the TBP indicating that the assigned atoms were incorrectly located (*i.e.* the assigned equatorial bond lengths were too short). Furthermore, a large negative peak (9.6σ) is observed for the central coordinating atom, indicating that the true atomic species is lighter than phosphorus.

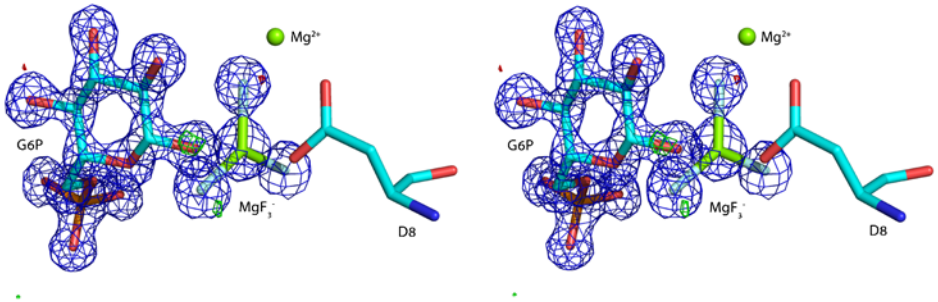

Fig. S5. Stereoview of the electron density maps for the β-PGM active site in 1o08 with MgF_3^- replacing PO_3^- in the model. The MgF_3^- moiety was placed in difference Fourier maps calculated from a model containing G6P as the only bound ligand and then refined against the downloaded structure factors. $2F_o - F_c$ density is shown as a *blue mesh* contoured at 1.5σ, difference density ($F_o - F_c$) is shown as *green and red meshes* contoured at +3σ and −3σ, respectively. MgF_3^- fits the density very well and there are no significant peaks in the difference Fourier map, confirming MgF_3^- as the correct trigonal planar model for the observed density.

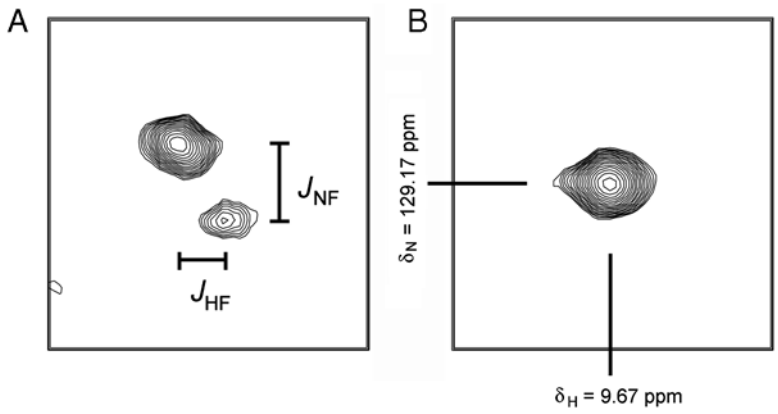

Fig. S6. Identical regions of ^1H, ^{15}N HSQC spectra recorded (*A*) without and (*B*) with ^{19}F decoupling showing the backbone amide resonance of A115 in the PGM-MgF_3-G6P-TSA complex. In (*A*), the HN peak is split horizontally by the $^1H - ^{19}F$ coupling ($J_{HF} = 36$ Hz) and vertically by the $^{15}N - ^{19}F$ coupling ($J_{NF} = 24$ Hz) through the hydrogen bond to F_B of the MgF_3^- moiety. All *J* measurements have an associated uncertainty of ±4 Hz. Similar *J*-coupling patterns are also observed for the backbone amide group of D10 ($J_{HF} = 45$ Hz, $J_{NF} = 22$ Hz), which is hydrogen bonded to F_A. Analogous *J*-coupling values for the other complexes are as follows: PGM-MgF_3-phosphonate-TSA, D10 $J_{HF} = 47$ Hz and $J_{NF} = 34$ Hz, A115 $J_{HF} = 43$ Hz and $J_{NF} = 27$ Hz; PGM-MgF_3-2deoxyG6P-TSA, D10 $J_{HF} = 53$ Hz and $J_{NF} = 34$ Hz, A115 $J_{HF} = 59$ Hz and $J_{NF} = 36$ Hz. In (*B*), these *J*-coupling patterns collapse to an average position in an ^1H, ^{15}N HSQC spectrum recorded with ^{19}F decoupling in both ^{15}N and ^1H dimensions.

Table S1. Data processing and refinement statistics for the native β-PGM and the PGM-MgF_3-G6P-TSA complex structures.

Structure	Native β-PGM	PGM-MgF_3-G6P-TSA	PGM-MgF_3-G6P-TSA Lλ
Space group	$P2_12_12_1$	$P2_12_12_1$	$P2_12_12_1$
Wavelength	0.933 Å	0.933 Å	1.77 Å
Unit cell dimensions (Å) a, b, c	53.3, 56.9, 75.4	37.6, 54.6, 105.2	37.1, 54.2, 104.1
Resolution range (Å)	20–1.55	20–1.3	20–2.0
Number of unique reflections	28,532	45,520	14,772
Multiplicity*	2.4 (2.0)	2.5 (1.8)	9.7 (9.9)
Completeness*† (%)	84.3 (43.1)	84.8 (47.2)	99.6 (98.8)
Rmerge*‡	0.06 (0.35)	0.06 (0.24)	0.09 (0.27)
σ*	10.7 (2.1)	8.5 (2.7)	15.9 (7.4)
Wilson B factor	19.2 Å^2	11.7 Å^2	18.9 Å^2
Water molecules	309	202	
R-factor§(%)	17.6	17.3	
Free R-factor¶(%)	20.8	19.2	
RMS deviations:			
Bonds (Å)	0.02	0.011	
Angles (°)	1.686	1.501	

*Statistics for the highest resolution bin (1.63–1.55 Å for the native β-PGM structure, 1.37–1.30 Å for the PGM-MgF_3-G6P-TSA complex structure and 2.11–2.0 Å for the long wavelength data set) are shown in parentheses.

†The completeness is low in the high resolution bins for the native and PGM – MgF_3 – G6P – TSA structures as these data were only recorded in the corners of the detector.

‡ $R_{\text{merge}} = \Sigma_h \Sigma_i |I(h) - I(h)_i| / \Sigma_h \Sigma_i I(h)_i$, where I(h) is the mean weighted intensity after rejection of outliers.

§ $R = \sum_{hkl} ||F_{obs}| - k|F_{calc}|| / \sum_{hkl} |F_{obs}|$, where F_{obs} and F_{calc} are the observed and calculated structure factor amplitudes.

¶ $R_{\text{free}} = \sum_{hkl \subset T} ||F_{obs}| - k|F_{calc}|| / \sum_{hkl \subset T} |F_{obs}|$, where F_{obs} and F_{calc} are the observed and calculated structure factor amplitudes and T is the test set of data omitted from refinement (5% in this case).

Table S2. Observed peak heights in the anomalous difference Fourier calculated using anomalous differences derived from data collected at a wavelength of 1.77 Å ($E = 7$ keV) with phases from a refined model. The peak heights of the sulfur atoms are lower than might be expected as the methionine residues that bear them are relatively mobile (reflected in the B factor). No peaks were observed in the positions corresponding to the locations of the magnesium atoms, the anomalous scattering factor being much smaller than for phosphorus or sulfur.

Peak height in anomalous difference Fourier (rms)	Location	$\Delta f''$ of element at $E = 7$ keV (electrons)	B factor (Å^2)
7.1	P6 of G6P	0.56	9.2
6.4	S of M126	0.72	12.9
4.7	S of M83	0.72	23.0
3.9	S of M1	0.72	24.5
-	Mg (catalytic)	0.23	11.9
-	Mg (MgF_3^-)	0.23	13.2